



Experimental investigation of surface integrity after wire electro-discharge machining of Ti–6Al–4V

DANIAL GHODSIYEH^{1,*}, SALEH AKBARZADEH¹, SUDIN IZMAN² and MONA MORADI³

¹Department of Mechanics, Isfahan University of Technology, Isfahan 84156-83111, Iran

²Department of Materials, Manufacturing and Industrial Engineering, Faculty of Mechanical Engineering, Universiti Teknologi Malaysia, Skudai, Malaysia

³Department of Mechanics and Aerospace, Politecnico di Torino, 10129 Turin, Italy

e-mail: danial.ghodsiyeh@gmail.com; s.akbarzadeh@cc.iut.ac.ir; izman@mail.fkm.utm.my; mona.moradi1988@gmail.com

MS received 6 February 2018; revised 27 November 2018; accepted 15 July 2019; published online 19 August 2019

Abstract. This article presents the relationship of machining parameters containing pulse-on time (T_{on}), pulse-off time (T_{off}), peak current (IP) and servo voltage (SV) on surface integrity characteristics, including white layer thickness (WLT), heat-affected zone (HAZ) and surface crack density (SCD) and also on material removal rate (MRR), after wire electric discharge machining of Ti–6Al–4V. Taguchi’s method was utilized to design the experiments, and response surface methodology (RSM) was employed for developing the empirical models. Results indicated that T_{on} and IP played a significant role on surface integrity characteristics. In addition, the microstructure of selected machined samples was analysed using a field emission scanning electron microscope (FESEM) and energy-dispersive X-ray (EDX) analysis. Accuracy of models was examined using residual analysis and confirmation runs. Finally, multi-response optimization of process parameters was obtained using desirability approach. Results can be used to improve the quality of the machined workpiece significantly to fulfil the requirements of the various industries. The novelty of this research is mainly investigation and multi-response optimization of all the surface integrity characteristics at the same time.

Keywords. Wire EDM; HAZ; surface crack density; white layer thickness; surface texture; RSM.

1. Introduction

Wire electrical discharge machining (WEDM) is a thermo-electrical process in which material is eroded by a series of sparks between the workpiece and the wire electrode (tool) [1]. The workpiece and wire are immersed in a dielectric fluid for cooling purposes and for cleaning debris. An advantage of this process is that workpiece and electrode are not in contact, allowing materials with different hardness values to be cut as long as they conduct electricity [2]. Wire movement is numerically controlled to achieve desired three-dimensional shape and high accuracy of the workpiece. This makes WEDM one of the best choices for precision machining, particularly for “superhard” materials and complex shapes [3].

It is a well-known fact that because of the various process variables, complexity and stochastic nature of WEDM process, achieving optimum performance criteria, even for a skilled operator, is extremely difficult [4, 5]. This problem becomes more complicated for hard material workpieces, such as titanium alloys.

Ti–6Al–4V belongs to the group of alpha–beta titanium alloys. Compared with steel, it is five times more corrosion-resistant. This material has a relatively high melting temperature, low thermal conductivity and high electrical resistivity compared with other common materials. Combination of high strength to weight ratio, excellent mechanical properties, corrosion resistance, high elastic stiffness and low density has made Ti–6Al–4V alloy the best choice for many critical applications. Reports indicate that it has been widely used in aerospace, military and commercial applications [6, 7]. Although WEDM is among the best choices for cutting Ti–6Al–4V, a major problem is huge thermal stress produced in the process. This thermal stress is created with energy discharge in the sparks bombarded of sample surface during machining process. This stress causes three major phenomena on the surface of specimen, including white or recast layer, surface crack and heat-affected zone (HAZ).

In WEDM, each spark melts a small portion of the workpiece. While a portion of this molten material is flushed away with dielectric, the remaining part rapidly re-solidifies to form a surface layer, known as recast or white layer. This white layer is in direct contact with the environment and the micro-cracks are mostly restricted to this

*For correspondence

Table 1. Literature review (tabular form).

No.	Investigator	Material used	Experimental design technique	Input parameters considered	Output (response)	Findings of the study
1	[10]	Pure titanium	Box–Behnken design, RSM, desirability function	Pulse-on time, pulse-off time, peak current, wire tension, wire feed, spark gap voltage	Cutting rate, dimensional deviation, surface roughness, wire wear ratio	Pulse-on time, pulse-off time and peak current are the major factors affecting MRR, WW ratio and dimensional deviation
2	[11]	Pure titanium	Taguchi design experiment	Pulse-on time, pulse-off time, peak current, wire tension, wire feed, spark gap voltage	Surface integrity and material transfer characteristics	Pulse-on time, pulse-off time and peak current are the major factors affecting surface integrity and wire rupturing
3	[12]	Pure titanium	Box–Behnken design, RSM, desirability function	Pulse-on time, pulse-off time, peak current, wire tension, wire feed, spark gap voltage	Material removal rate, wire wear ratio and surface roughness	Pulse-on time, peak current and interaction between them are the major factors affecting material removal rate, wire wear ratio and surface roughness
4	[13]	Die steel	RSM-rotatable central composite design	Pulse-on time (rough cut), pulse-on time (trim cut), cutting speed	White layer depth	White layer depth increases with increasing pulse-on time during rough cut and decreases with increasing pulse-on time during trim cutting
5	[8]	Nimonic 80A	Taguchi's L27 orthogonal array, non-linear regression analysis	Pulse-on time, pulse-off time, peak current, wire tension, wire feed, spark gap voltage	Surface integrity, material removal rate and wire wear ratio	Pulse-on time and pulse-off time major factors affecting material removal rate, $T_{on}-T_{off}$ and $T_{on}-IP$ interaction major factors affecting wire wear ratio
6	[14]	Pure titanium	Taguchi design experiment, RSM	Pulse-on time, pulse-off time, pulse current and spark gap voltage	Surface crack density and recast layer thickness	Pulse-on time, pulse-off time and peak current are the major factors
7	[15]	Inconel 625	Taguchi design experiment, RSM	Pulse-on time, pulse-off time, spark gap voltage and wire feed	Cutting speed, gap current and surface roughness	Pulse-on time and pulse-off time are significant while spark gap voltage is the least significant
8	[16]	Ti–6Al–4V	RSM, NSGA-II	Pulse-on time, pulse-off time, pulse current	Material removal rate, sparking gap, white layer thickness and wire type	Wire type is the major factor affecting white layer and material removal rate followed by pulse-on time and peak current

layer. White layer at the surface of the workpiece machined by WEDM is extremely susceptible to fatigue failure [8]. Below the recast layer, there is HAZ, which depending on the chemical mixture of the workpiece can be a composition of several secondary layers. The HAZ may also contain an altered microstructure, tensile stresses, micro-cracks, impurities and other undesirable features, subjected to premature part failure under operation [9].

Furthermore, the intense heat generated with each discharge during machining results in local severe temperature gradients on the machined surface. Upon discharge cessation, surface layers quickly cool, developing a residual tensile stress sufficient to produce cracks on the machined surfaces. Among these surface defects, cracking is the most

significant since it reduces material resistance to fatigue and corrosion, especially under tensile loading condition.

A comprehensive literature review has been performed on various aspects of WEDM process and is summarized in table 1. Although several attempts were made to understand the mechanism of formation and properties of the white layer and HAZ, it is evident from the literature review that few research works [10–16] have been conducted to model the process by correlating the dominant input parameters with the white layer and HAZ depth as the machining performance, especially since it is not easy to identify and measure HAZ.

Multi-objective parametric optimization using mathematical models which developed by the response surface

Table 2. Cutting parameters and their levels.

Coded factor	Machining parameters	Symbol	Levels		
			−1	0	1
A	Pulse-on time (μs)	T_{on}	6	8	10
B	Pulse-off time (μs)	T_{off}	4	6	8
C	Peak current (A)	IP	16	24	32
D	Servo voltage (V)	SV	30	40	50
Constant parameters			Description		
Machining voltage (V)			80		
Wire speed (m/min)			10		
Wire tension (g)			600		
Flushing pressure (bar)			50		
Tool polarity			Negative		
Dielectric fluid			Deionized water		
Wire material			Zinc-coated brass		

methodology (RSM) and Analysis of Variance (ANOVA) is used in different studies such as [17] and proved to be specially useful in different machining processes.

The objective of this study is modelling and optimizing WEDM of titanium alloy. The focus is on surface integrity of specimen containing surface topography, HAZ, surface crack density and material migration. Results are particularly useful to produce high-quality workpiece in terms of surface texture for scientists and engineers to determine which subset of the process variable has maximum influence on the process performance. In addition, there is a tradeoff between material removal rate and surface integrity parameters.

2. Experimental procedure

Experimental trials were performed using a WEDM linear motor 5-ax –CNC Sodick series AQ537L. The experimental set-up is as follows: zinc-coated brass wire of 0.25 mm diameter is employed as the electrode. Composition of the titanium-based alloy (Ti–6Al–4V) is as follows: C = 0–0.08%, Fe = 0–0.25%, Al = 5.5–6.76%, O = 0–0.2%, N = 0–0.05%, V = 3.5–4.5%, H = 0–0.375%, balance Ti). RSM approach was used to design the experiments and optimization process. The input parameters and initial settings were selected based on the existing literature and some initial investigations (table 1). Four significant factors of machining process are considered in this study: pulse-on time, pulse-off time, peak current and servo voltage. The low, middle and high levels of these four parameters are presented in table 2. Design Expert 7.0.0.0 software was utilized to optimize and analyse data.

In the trials, 2^k factorials with central composite face-centred design were considered as full factorial design (where $k = 4$); therefore, $n_c = 2^k = 16$, corner points at +1 and −1 levels. Also, the centre points at zero level were

repeated four times. Consequently, the total number of experimental trials was 20.

In these experiments, the order of the experiment was random because ANOVA requires observations or errors to be independently distributed random variables. By properly randomizing the experiment, the effects of extraneous factors or confounding variables that may be present are averaged out. Confidence level of 95% ($\alpha = 0.05$) was used throughout analysis of the experiment and Fisher's F -test verified the statistical significance of the model [18].

In each trial, a 10-mm length of cutting was made on 10-mm thickness of the workpieces. MRR value is obtained by the following equation:

$$\text{MRR} = (W_b - W_a)/(T_m \rho) \text{ (mm}^3/\text{s)} \quad (1)$$

where W_b and W_a are mass of workpiece material before and after machining (g), respectively. T_m is machining time (s) and ρ is the density of workpiece material (Ti–6Al–4V, 0.00443 g/mm³).

In this study, surface integrity was analysed and measured using a field emission scanning electron microscope (FESEM) (Philips XL40), which was integrated with an energy-dispersive X-ray (EDX) spectrometer. Samples were thoroughly cleaned with acetone and were mounted, exposing to an area of approximately 2 mm × 25 mm of resin and hardener in a mould. The mounted specimens were then ground and polished. Polishing was performed to have mirror finish on the transverse section and subsequently these faces were etched with Kroll's reagent (2% hydrofluoric acid + 10% nitric acid + 88% water) for 10–15 s. Henceforth, these samples were observed with the aid of FESEM. The white layers from the photographs were easily identified. The depths of white layers were measured carefully from the micrographs. Averages of readings were taken for each experimental run. Figure 1 shows cross-sectional view for measuring white layer of workpiece for standard order numbers 2, 9, 20 and 22. Measurements for

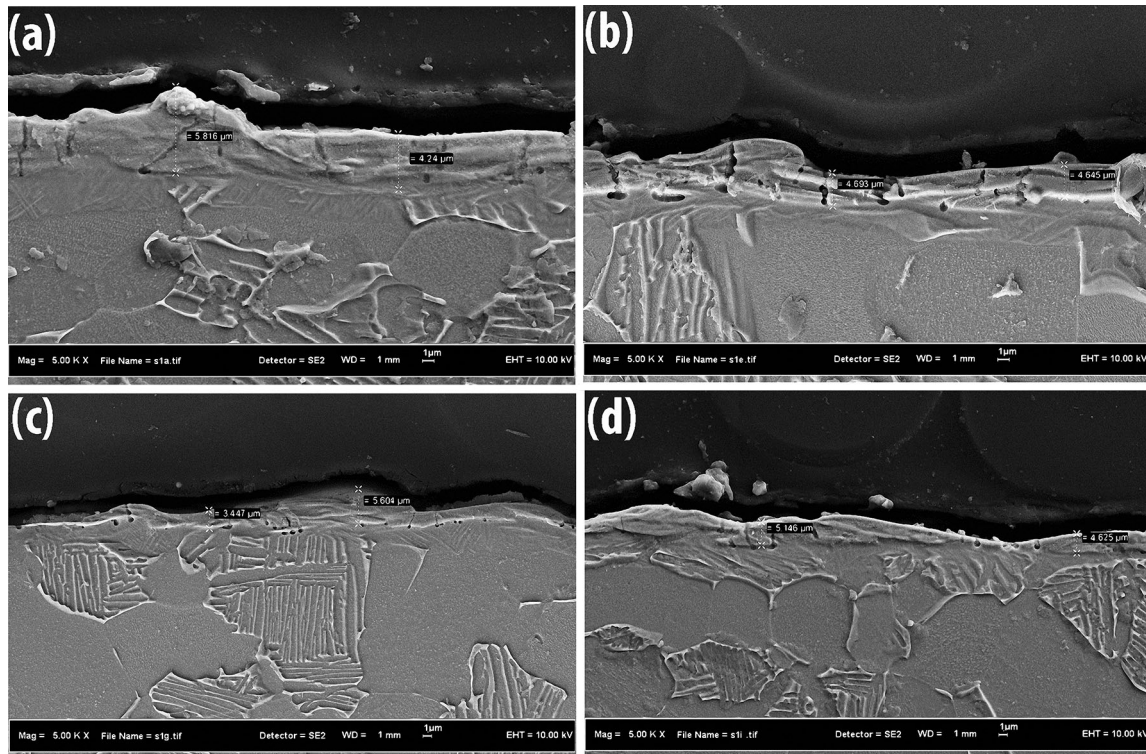


Figure 1. Cross-sectional views showing white layer standard order numbers 2 (a), 9 (b), 20 (c) and 22 (d).

HAZ identification were carried out with different magnifications (1000 \times and 5000 \times), and averages of readings were taken for each experimental run. Figure 2 shows a cross-sectional view of the workpiece for measuring HAZ standard order numbers 2, 6, 19 and 27.

Surface crack density (SCD) is calculated from the following equation:

$$\text{SCD} = \text{TLC}/A \quad (1)$$

where SCD is surface crack density, TLC is total length of crack in μm and A is the reference area of micrograph in μm^2 . Since length of cracks is obviously more important than number of cracks and it is not easy to measure a crack in terms of width, length, depth or by amount of cracking [19], this research defines a “surface crack density”, i.e. the total length of cracks (μm) in reference area (μm^2), to evaluate the severity of cracking. Measurements were done by importing the FESEM micrographs into Carl Zeiss Axio-vision Rel.4.8 software. Different magnifications (from 500 \times to 5000 \times) were used to observe the machined surfaces. Especially for curved cracks, higher magnification can be used for more accurate measurements. The measurement precision for 10.0 kV is 10 nm. The reference area defined for all micrographs was considered $8800\mu\text{m}^2/\mu\text{m}^2$. The crack measurements of standard order numbers 13 and 22 are shown in figure 3.

3. Results and discussion

This part consists of experimental results, expressing the effect of four control factors consisting of T_{on} , T_{off} , IP and SV on different responses, including SCD, HAZ and WLT, by full factorial design. Results of experiments were used to formulate the RSM models of each response.

In these experiments, high flushing pressure is absolutely necessary for rough machining due to low thermal conductivity of titanium alloy; otherwise, the short-circuit phenomenon will cause wire breakage. Due to frequent wire breakages in pilot experiments, flushing pressure for all the experiments was increased from 40 to 50 bar. Table 3 shows the experimental results in standard (Std) order number.

Table 4 shows ANOVA for surface crack density. According to this table, model F -value is 111.15, which indicates that it is significant. Probability that noise causes “model F -value” is just 0.01% in the case of “Prob > F ”, which is smaller than 0.0500; this implies that the model terms are significant. Therefore, (A) T_{on} , (C) IP and (D) SV are principal terms, and the other model terms can be considered to be insignificant. The model is likely to be improved when the insignificant model terms are omitted. According to the “curvature F -value” of 20.79, curvature in the design space is significant. For surface crack density the second-order model can be achieved by applying

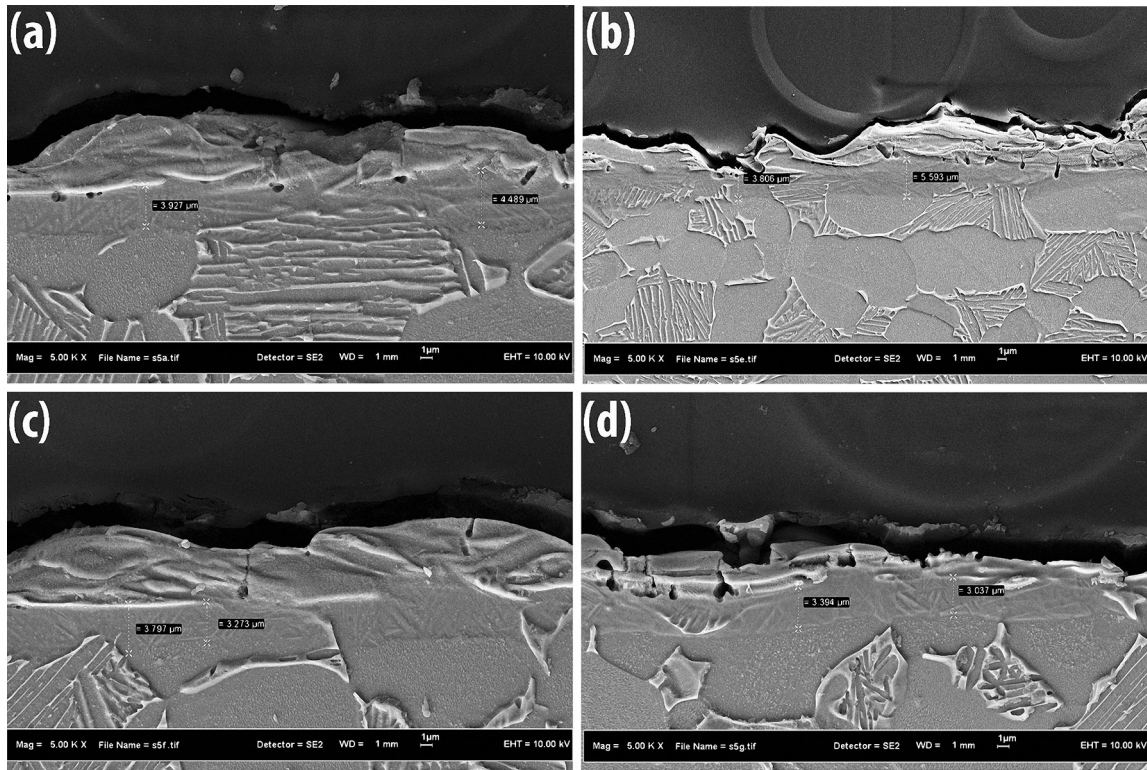


Figure 2. Cross-sectional views showing heat-affected zone (HAZ) standard order numbers 2 (a), 6 (b), 19 (c) and 27 (d).

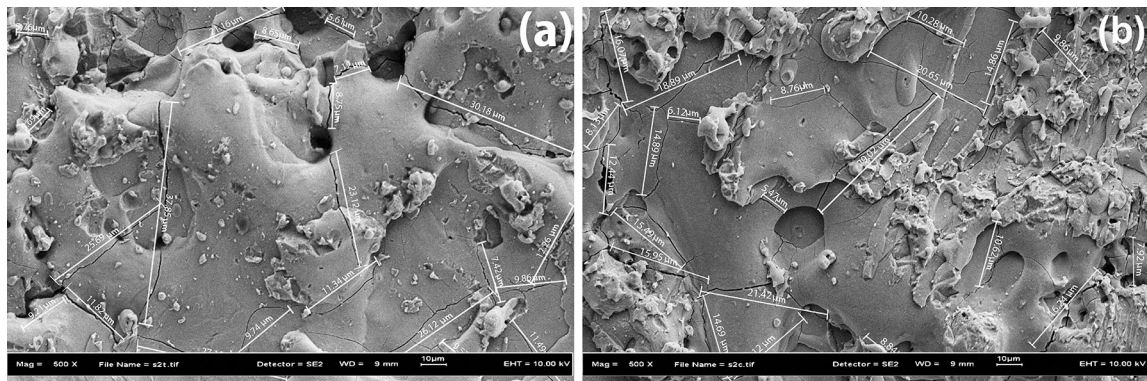


Figure 3. Demonstration of micro-cracks in different parametric conditions: (a) Exp. 13, $TLC = 325.52 \mu\text{m}$, $A = 8800 \mu\text{m}^2$, $SCD = 0.037 \mu\text{m}/\mu\text{m}^2$, $MRR = 0.3388 \text{ mm}^3/\text{s}$ and (b) Exp. 15, $TLC = 301.73 \mu\text{m}$, $A = 8800 \mu\text{m}^2$, $SCD = 0.0343 \mu\text{m}/\mu\text{m}^2$, $MRR = 0.3212 \text{ mm}^3/\text{s}$.

augment experiments. ‘‘Lack of fit F -value’’ of 0.85 reveals that it is not significantly related to the pure error, and it is a confirmation that the model is properly matched with the results.

Similar to the ANOVA table for the surface crack density, two more ANOVA tables for other responses have been analysed and a summary of the significant factors and the contribution percentage for each factor are presented in table 5.

In case of significant system curvature, the relation between parameters and the factor is not linear, and polynomials of higher degree must be used instead of first-order model. Therefore, in this study, second-order model is considered. According to table 5, ANOVA analysis reveals the significance of curvature test for all responses; therefore, the second-order model will be applicable and suitable for mentioned responses in table 5. Finally, an RSM-designed model – central composite design (CCD) – was

Table 3. Experimental results.

Std order	Machining parameters				Response factors			
	T_{on} (μs)	T_{off} (μs)	IP (A)	SV (V)	SCD (μm/μm ²)	HAZ (μm)	WLT (μm)	MRR (mm ³ /s)
1	6	4	16	30	0.0065	3.51	4.088	0.198
2	10	4	16	30	0.0102	4.21	5.028	0.259
3	6	8	16	30	0.0052	3.42	3.839	0.178
4	10	8	16	30	0.0081	4.02	4.464	0.215
5	6	4	32	30	0.0301	3.79	4.951	0.262
6	10	4	32	30	0.0442	4.7	5.879	0.342
7	6	8	32	30	0.0276	3.65	4.754	0.225
8	10	8	32	30	0.0409	4.59	5.386	0.329
9	6	4	16	50	0.0078	3.38	4.669	0.245
10	10	4	16	50	0.0256	3.88	5.737	0.308
11	6	8	16	50	0.0074	3.35	4.582	0.235
12	10	8	16	50	0.0174	3.85	5.137	0.287
13	6	4	32	50	0.037	3.56	5.539	0.339
14	10	4	32	50	0.0488	4.32	6.015	0.387
15	6	8	32	50	0.0343	3.51	5.428	0.321
16	10	8	32	50	0.0466	4.24	5.912	0.371
17	8	6	24	40	0.0185	3.76	4.257	0.319
18	8	6	24	40	0.0124	3.62	5.238	0.301
19	8	6	24	40	0.0145	3.54	3.947	0.299
20	8	6	24	40	0.0201	3.74	4.525	0.312

Table 4. ANOVA for the surface crack density.

Source	Sum of squares	df	Mean square	F-value	Prob > F	
Model	3.692e-3	3	1.231e-3	111.15	<0.0001	Significant
A	4.612e-4	1	4.612e-4	41.66	<0.0001	
C	3.061e-3	1	3.061e-3	276.48	<0.0001	
D	1.697e-4	1	1.697e-4	15.32	0.0014	
Curvature	2.302e-4	1	2.302e-4	20.79	0.0004	Significant
Residual	1.661e-4	15	1.107e-5			
Lack of fit	1.284e-4	12	1.070e-5	0.85	0.6400	Not significant
Pure error	3.771e-5	3	1.257e-5			
Cor. total	4.088e-3	19				

Table 5. Contribution percentages of significant factors.

Response	Pulse on (A)	Pulse off (B)	Peak current (C)	Servo voltage (D)	Curvature
SCD	11.28%	0.79%	74.88%	4.15%	5.63%
WLT	23.80%	4.22%	29.17%	15.66%	13.29%
HAZ	66.64%	1.08%	15.70%	6.83%	4.74%
MRR	24.39%	3.2%	42.04%	23.39%	3.55%

applied for developing the second-order models. For this purpose, eight experiments were carried out on axial points, as discussed in table 6 ($2k = 8$). For the new experiments, new block was designed to examine the repeatability of process because these experiments were conducted with different conditions, i.e., a different operator on a different day. Furthermore, Eq. (2) was used

to calculate and establish the second-order model through ANOVA table:

$$Y_U = b_0 + \sum_{i=1}^K b_i X_i + \sum_{i=1}^K b_{ii} X_i^2 + \sum_{j>i}^K b_{ij} X_i X_j + \dots + e \tag{2}$$

where i is the linear coefficient, j is the quadratic coefficient, b is the regression coefficient, k is the number of studied and optimized factors in the experiment and e is the random error. ANOVA was used in order to estimate the validity of the regression model. F -ratio was employed to determine the significance of the model regarding variance of all terms at appropriate level of α [18]. Table 6 illustrates experimental results based on CCD.

To test the significance of the individual model coefficients, the model may be optimized by adding or removing coefficients through backward elimination, forward

Table 6. Experimental results for augment CCD.

Std order	Machining parameters				Response factors			
	T_{on} (μs)	T_{off} (μs)	IP (A)	SV (V)	SCD (μm/μm ²)	HAZ (μm)	WLT (μm)	MRR (mm ³ /s)
21	6	6	24	40	0.0044	3.386	4.126	0.2325
22	10	6	24	40	0.0423	3.705	4.885	0.2995
23	8	4	24	40	0.0214	3.657	4.816	0.2732
24	8	8	24	40	0.0114	3.445	4.322	0.2291
25	8	6	16	40	0.0088	3.575	3.764	0.2165
26	8	6	32	40	0.0356	4.067	5.612	0.3592
27	8	6	24	30	0.0105	3.216	4.616	0.2153
28	8	6	24	50	0.0224	3.805	5.319	0.2639

addition or stepwise elimination/addition/exchange [20]. The probability of significance, known as the *P*-value, was initially determined. The effect of the independent variable is significant if the *P*-value is equal to or less than the selected α -level, and the insignificant variables are those with *P*-values greater than the selected α -level [21]. It should be noted that the effects of interactions among pairs of variables can be significant even though one variable effect is not individually significant; hence the insignificant individual variables were not considered in backward elimination.

Tables 7–10 are ANOVA results of the reduced quadratic model for responses by implementing the backward elimination procedure with α equal to 0.05.

For all models, the block effects are not significant; this implies that the mentioned different conditions do not affect the results and the process is repeatable.

Since all R^2 -values are close to unity, the results are satisfactory. The difference between values of adjusted ($Adj. R^2$) and predicted ($Pred. R^2$) – which is smaller than 0.2 – shows that they are in agreement. Since adequate predictions (adeq. precision) of all models are more than 4, the signals of the models are appropriate. The *S/N* ratios,

which were presented as adequate precisions, are 19.804, 16.413 and 17.402, which indicates that models are desirable to navigate design space. Equations (3), (4), (5) and (6) are final empirical models in terms of actual factors for surface crack density (SCD), HAZ, white layer thickness (WLT) and material removal rate (MRR), respectively:

$$HAZ = +4.11059 + 0.16561T_{on} - 0.15325IP - (6.76667e-3)SV + 3.66024e-003(IP)^2, \quad (3)$$

$$SCD = +0.052351 - 0.026042T_{on} + (1.72292e-3)IP + (3.55556e-4)SV + 1.84255e-3(T_{on})^2, \quad (4)$$

$$WLT = +9.48402 + 0.17964T_{on} - 0.0805T_{off} + 0.056722IP - 0.39216SV + 5.27234e-3(SV)^2, \quad (5)$$

$$MRR = -0.48408 + 0.015603T_{on} - 0.00620556T_{off} + 0.00550139IP + 0.024674SV - 0.000271404(SV)^2. \quad (6)$$

Table 7. ANOVA for reduced response surface quadratic model for surface crack density.

Source	Sum of squares	df	Mean square	<i>F</i> -value	Prob > <i>F</i>	
Block	7.242e-5	1	7.242e-5			Insignificant
Model	4.754e-3	4	1.188e-3	42.58	<0.0001	Significant
A	8.515e-4	1	8.515e-4	30.51	<0.0001	
C	3.420e-3	1	3.420e-3	122.52	<0.0001	
D	2.276e-4	1	2.276e-4	8.15	0.0092	
A ²	2.553e-4	1	2.553e-4	9.15	0.0062	
Residual	6.141e-4	22	2.791e-5			
Lack of fit	5.763e-4	19	3.033e-5	2.41	0.2554	Not significant
Pure error	3.771e-5	3	1.257e-005			
Cor. total	5.440e-3	27				
Std. dev.	5.283e-3		R^2	0.8856		
Mean	0.022		Adj. R^2	0.8648		
C.V.%	23.86		Pred. R^2	0.7942		
PRESS	1.105e-3		Adeq. precision	19.804		

Table 8. ANOVA for reduced response surface quadratic model for heat-affected zone.

Source	Sum of squares	df	Mean square	F-value	Prob > F	
Block	0.28	1	0.28			Insignificant
Model	2.90	4	0.72	27.30	<0.0001	Significant
A	1.97	1	1.97	74.50	<0.0001	
C	0.58	1	0.58	21.88	0.0001	
D	0.082	1	0.082	3.11	0.0917	
C ²	0.26	1	0.26	9.73	0.0050	
Residual	0.58	22	0.027			
Lack of fit	0.55	19	0.029	2.72	0.2232	Not significant
Pure error	0.032	3	0.011			
Cor. total	3.76	27				
Std. dev.	0.16		R ²	0.8323		
Mean	3.77		Adj. R ²	0.8018		
C.V.%	4.32		Pred. R ²	0.7348		
PRESS	0.92		Adeq. precision	16.413		

Table 9. ANOVA table for reduced response surface quadratic model for white layer thickness.

Source	Sum of squares	df	Mean square	F-value	Prob > F	
Block	0.47	1	0.47			Insignificant
Model	9.38	5	1.88	22.01	<0.0001	Significant
A	2.32	1	2.32	27.25	<0.0001	
B	0.47	1	0.47	5.47	0.0293	
C	3.71	1	3.71	43.47	<0.0001	
D	1.58	1	1.58	18.53	0.0003	
D ²	1.31	1	1.31	15.32	0.0008	
Residual	1.79	21	0.085			
Lack of Fit	0.88	18	0.049	0.16	0.9956	Not significant
Pure Error	0.91	3	0.30			
Cor. total	11.64	27				
Std. dev.	0.29		R ²	0.8398		
Mean	4.89		Adj. R ²	0.8016		
C.V.%	5.97		Pred. R ²	0.7425		
PRESS	2.88		Adeq. precision	17.402		

Table 10. ANOVA table for reduced response surface quadratic model for material removal rate.

Source	Sum of squares	df	Mean square	F-value	Prob > F	
Block	0.003777	1	0.003777			Insignificant
Model	0.074	5	0.015	57.08	<0.0001	Significant
A	0.018	1	0.018	67.23	<0.0001	
B	0.002773	1	0.002773	10.63	0.0037	
C	0.035	1	0.035	133.72	<0.0001	
D	0.016	1	0.016	60.56	<0.0001	
D ²	0.003462	1	0.003462	13.28	0.0015	
Residual	0.005475	21	0.002607			
Lack of fit	0.005199	18	0.0002889	3.14	0.1881	Not significant
Pure error	0.0002759	3	0.00009198			
Cor. total	0.084	27				
Std. dev.	0.016		R ²	0.9315		
Mean	0.28		Adj. R ²	0.9151		
C.V.%	5.78		Pred. R ²	0.8840		
PRESS	0.009268		Adeq. precision	29.044		

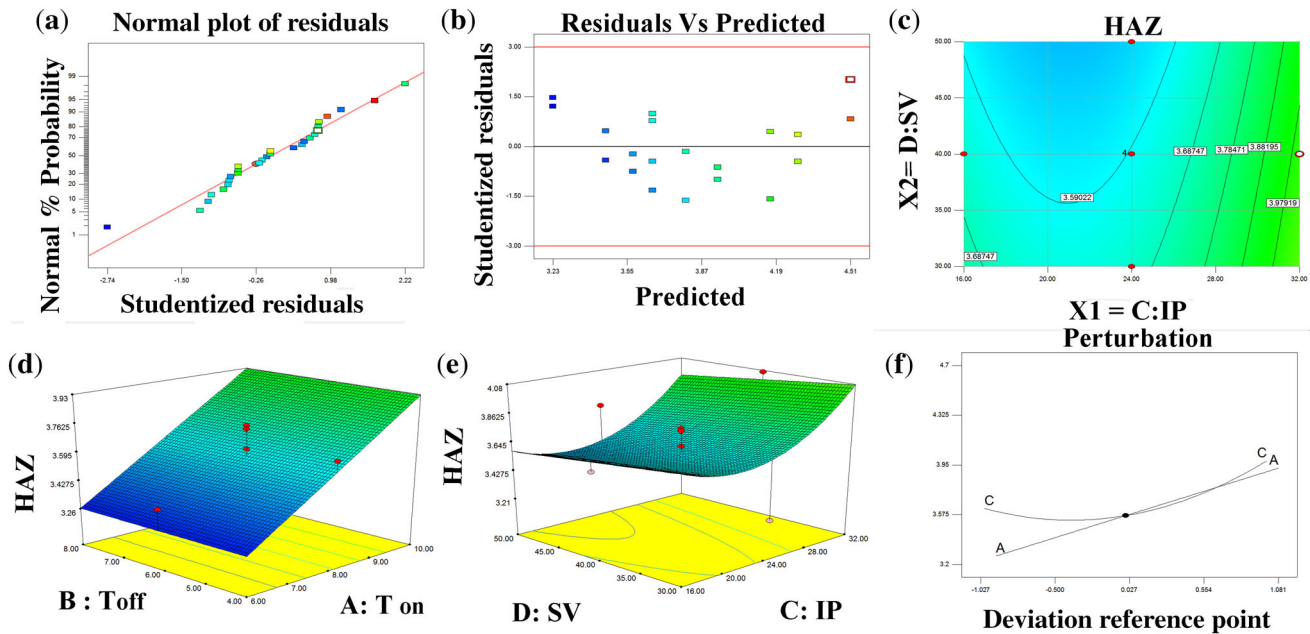


Figure 4. Response surface plot for heat-affected zone (HAZ): (a) normal probability plot of residuals; (b) residuals versus predicted; (c) contour plot; (d) interaction plot for T_{on} and T_{off} ; (e) interaction plot for IP and SV and (f) perturbation plot.

3.1 Haz

As mentioned previously, below white layer there is an altered layer named HAZ, which is caused by intense heat generated and rapid quenching during WEDM process. Low thermal conductivity reduces heat dispersion, which makes thermal stresses penetrate deeply in the material. Therefore, depth of HAZ produced by WEDM machining depends on thermal conductivity of workpiece and for titanium it is significantly larger than those for most of other commercial materials.

According to the normal probability plot in figure 4(a) the distribution of the residuals along the probability line is normal, indicating that the error distribution for all groups of data is almost homogeneous. In addition, according to residual versus predicted plot (b), all data presented are in the range, and no abnormal trends have observed. Figure 4(d)–(f) demonstrates that HAZ increases as T_{on} and IP increase. The reason is that with increase of discharge period, double and localized sparking are more frequent [22–24]. Due to low thermal conductivity of titanium, discharge period (T_{on}) is the most significant factor. Finally, it was found that SV has a lower significance and T_{off} does not have significant effect on the HAZ.

3.2 Surface crack density (SCD)

Crack formation is often associated with high thermal stresses and plastic deformation. Although machining parameters play a significant role in formation of micro-cracks, several material properties such as tensile strength,

thermal conductivity, thermal expansion coefficient and Young’s modulus are also important [25].

Figure 5(a)–(c) shows the normal probability plot of residuals and residual versus predicted plots for SCD. It was observed that the residuals generally fall on a straight line, implying that the errors are homogeneously distributed. From figure 5(d)–(f) it can be concluded that IP is the most significant factor that affects SCD. IP and energy of each discharge are in direct relationship and higher energy produces wider and deeper craters, which affect crack formation in the surface. This outcome agrees with the results obtained for SCD reported by Kumar *et al* [11] and Lee and Tai [19], which express that IP and T_{on} have major effects on SCD. Furthermore, Hascalik and Caydas [26] investigated the machining characteristic of AISI D5 tool steel in WEDM process experimentally. They found that intensity of process energy affects the amount of WLT and surface roughness as well as micro-cracking.

3.3 White layer thickness (WLT)

White layer is defined as material melted by electrical discharge and re-solidified on the workpiece surface.

According to the normal probability plot of residuals in figure 6(a) and residual versus predicted plot in figure 6(b) the error distribution is normal and plots seem to be structureless, which satisfy the assumptions. According to figure 6(d)–(f), curvature is significant for WLT in SV– T_{on} interaction plot. White layer increases significantly as the machining condition is stable in some SV. In addition, IP is the most significant factor that affects white layer, while T_{on} and SV play similar

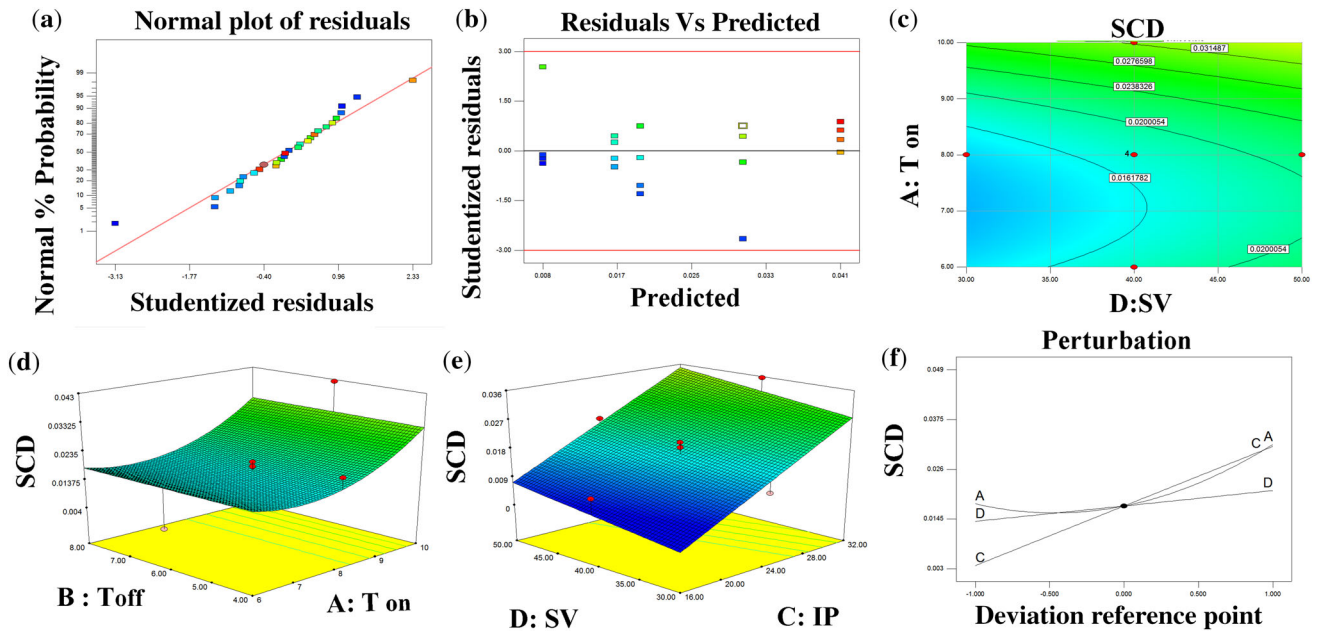


Figure 5. Response surface plot for surface crack density (SCD): (a) normal probability plot of residuals; (b) residuals versus predicted; (c) contour plot; (d) interaction plot for T_{on} and T_{off} ; (e) interaction plot for IP and SV and (f) perturbation plot.

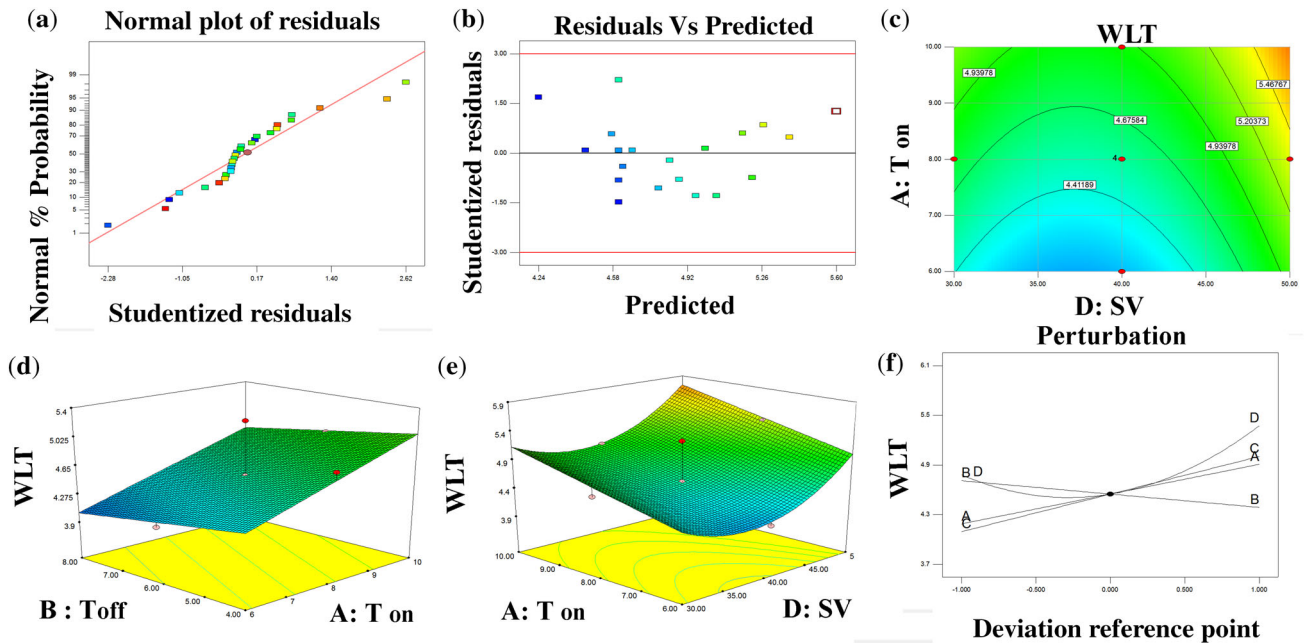


Figure 6. Response surface plot for white layer thickness (WLT): (a) normal probability plot of residuals; (b) residuals versus predicted; (c) contour plot; (d) interaction plot for T_{on} and T_{off} ; (e) interaction plot for SV and T_{on} and (f) perturbation plot.

role in this response. It was found that WLT is in direct relation with IP and T_{on} while it is in opposite relation with T_{off} . As T_{off} decreases there is not enough time for proper cleaning of debris and pollution in sparking gap, leading to occurrence of more sparks. Also, in low T_{off} time, heat dispersion decreases, causing more heat entrapment and melted material in the

surface, which produces thicker white layer. These results are in agreement with other research works as mentioned in the literature review [13, 15, 16]. Moreover, Ghodsiyeh *et al* [27] reported that IP and SV have more significant effects on the WLT than the pulse-on time and pulse-off time in WEDM machining of Ti-6Al-4V.

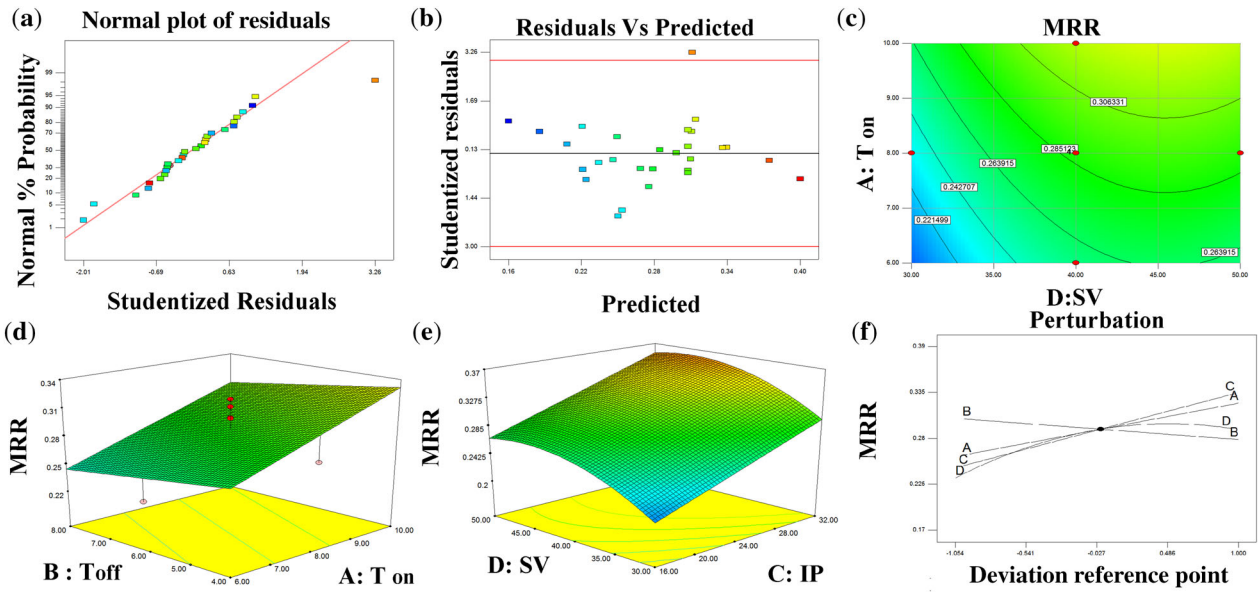


Figure 7. Response surface plot for white layer thickness (MRR): (a) normal probability plot of residuals; (b) residuals versus predicted; (c) contour plot; (d) interaction plot for T_{on} and T_{off} ; (e) interaction plot for SV and T_{on} and (f) perturbation plot.

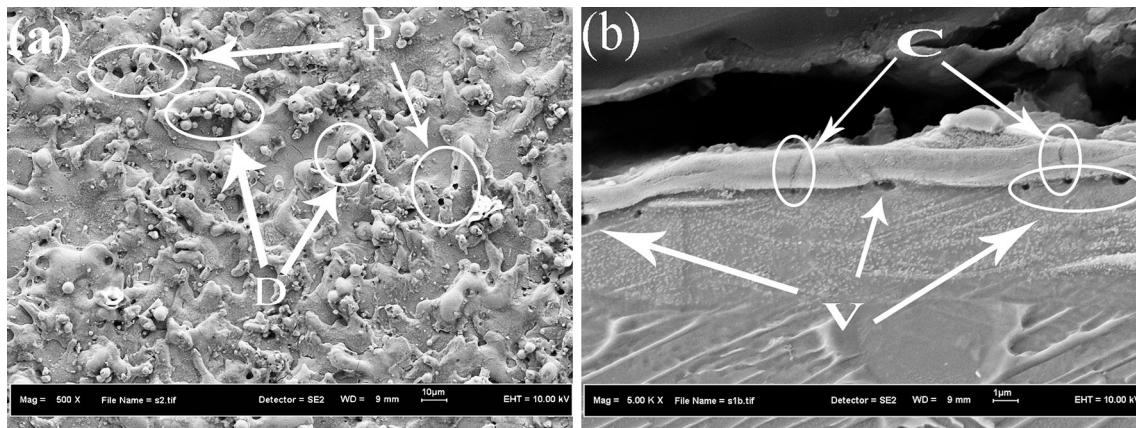


Figure 8. FESEM micrograph (a) and cross-sectional (b) view of Ti-6Al-4V after WEDM under the conditions of Std order no. 3 ($T_{on} = 6 \mu s$, $T_{off} = 8 \mu s$, IP = 16 A, SV = 30 V). C, crack; V, void; P, pockmarks and D, spherical debris.

3.4 Material removal rate (MRR)

Increasing the material removal rate will considerably increase the production rate by reducing the machining time.

According to the normal probability plot in figure 7(a) the distribution of the residuals along the probability line is normal, which shows that data are almost standardized. In addition, according to residual versus predicted plot in figure 7(b), all data presented are in the range, except run no. 26, which is slightly above the range, and no abnormal trends are observed.

Figure 7(d)–(f) establishes that MRR increases as T_{on} and IP increase. IP is the most significant factor. Increasing IP causes more electrical discharge energy to be imposed

into the machining gap and increases MRR. T_{on} and SV are less significant and T_{off} does not have significant effect on MRR.

3.5 Surface topography and material transformation analysis

Surface topography characteristics include shallow craters (SH.C), spherical particles, melted drops, globules of debris (D), voids (V) and cracks (C), which are created due to the high heat energy released followed by rapid cooling in WEDM process. These features can significantly affect properties of workpiece like fatigue life and tensile strength. In surface topography, cracks can be separated to

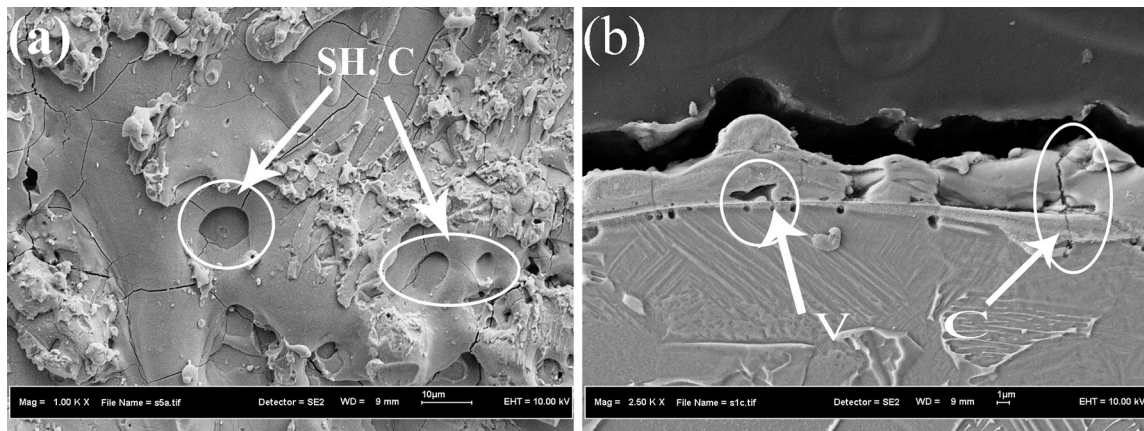


Figure 9. FESEM micrograph (a) and cross-sectional (b) view of Ti-6Al-4V after WEDM under the conditions of Std order no. 13 ($T_{on} = 6 \mu s$, $T_{off} = 4 \mu s$, $IP = 32 A$, $SV = 50 V$). SH.C, shallow craters and V, voids.

two different categories: surface cracks that normally exist in the white layer and penetrating cracks that penetrate more deeply into the original material. Penetrating cracks can play a significant role in failure modes of the components and service performance.

Figure 8 presents the FESEM surface topography characteristics produced by WEDM. A great amount of spherical debris and pockmarks are noticeable in this figure. This spherical debris may be solidified from the vaporized material or arise from splashing molten material that undergoes rapid water quenching. Micro-cracks are hardly found in this experiment due to low IP and T_{on} .

Figure 9 reveals that the surface topology consists of an uneven fused structure, globules of debris, shallow craters, voids and cracks. Because of high IP and SV in this experiment, the heat that was produced by the discharge is greater than in the previous experiments, and the size of craters is relatively larger. Cross-sectional view also shows deeper cracks in this experiment. Although these cracks are not deep enough to penetrate in the original material, they can cause crack initiation and propagation, especially under fatigue conditions, and also they affect surface roughness.

These figures demonstrate that the surface topography features increase as T_{on} and IP increase, while SV also has an important role. Increasing IP, as it is the most significant factor, causes more electrical discharge energy to be conducted into the machining gap [28], and formation of more voids, surface and penetrating cracks. In addition, with longer T_{on} , the available power between anode and cathode becomes greater, strengthening discharge energy, which facilitates melting and evaporation of materials [29–31]. As a result, a surface with higher porosity and debris is produced. Moreover, based on the manual of Sodic WEDM machine, as the servo voltage increases, sparking gap decreases, which means the machining condition is more stable and more severe. The study reported by Hascalik and Caydas [32] presents that the most significant parameters are pulse-on time and peak current for the surface integrity

of pure titanium, leading to deterioration of the surface texture, which is in agreement with the results of this study.

Finally, material transformation analysis was performed using EDX technique to identify the element composition of the machined samples. EDX analysis plots show how frequently an X-ray is received for each energy level. EDX spectrum shows peaks corresponding to the energy levels of received X-rays. Each of these peaks is unique for an atom and corresponds to a single element; this is the basic characteristic used by the FESEM machine to recognize all types of compositions in the specimen and produce a table of all materials as in figure 10.

From the EDX analysis obtained at accelerating voltage of 3 kV and shown in figure 10, the residuals of copper and zinc are detected in the machined samples. This may be due to melting and re-solidification of zinc-coated brass wire electrode transferred to the workpiece. EDX analysis in both samples shows existence of different types of dioxide, including titanium dioxide (TiO_2), aluminium dioxide (Al_2O_3) and vanadium dioxide (V_2O_5). These elements were observed due to existence of oxygen in the deionized water as dielectric fluid.

4. Confirmation runs and optimization

In order to verify the adequacy of the model and the developed mathematical equation, confirmation test was performed. Predicted values for confirmation tests were suggested by the Design Expert 7.0.0 software. Six experiments were conducted to determine the error of different models, and averages of errors are presented in table 11. The errors obtained from all responses are lower than 15% of allowable marginal error. It shows that all the empirical models are reasonably accurate due to the presence of actual responses in the range of prediction intervals.

Table 12 shows the principles of optimization used in Design Expert 7.0.0.0 software. Finally, table 13 presents

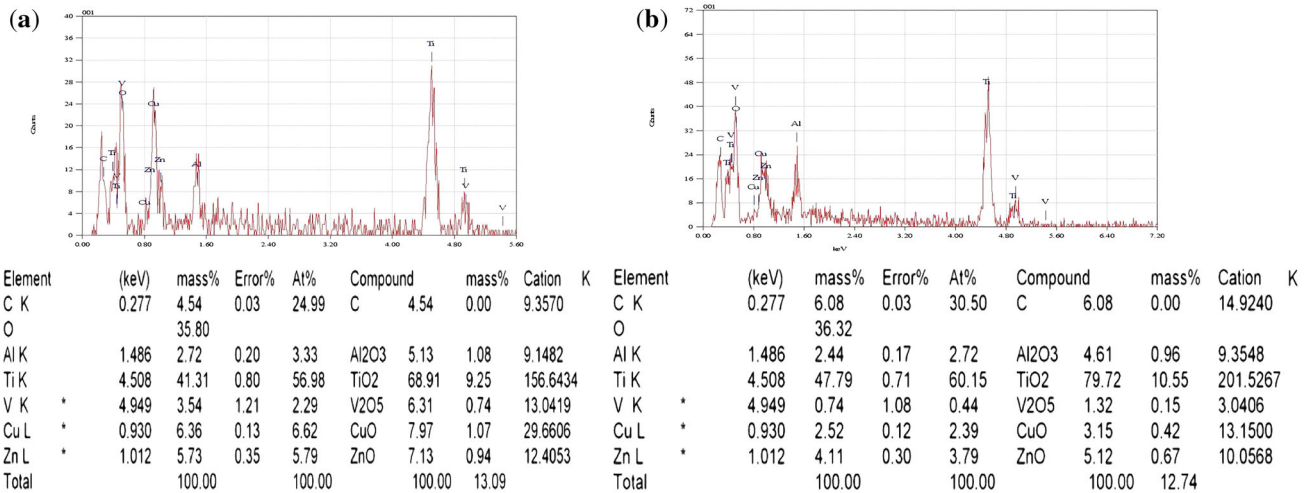


Figure 10. EDX analysis result of pure titanium after WEDM under conditions of Std order 2 (a) and 5 (b).

Table 11. Results of confirmation experiments.

Surface crack density	Heat-affected zone	White layer thickness	Material removal rate
10.65%	14.85%	6.42%	12.35%

the best combination of parameters to access each optimal condition using desirability approach. In this table, the results for all responses are in the optimum region,

and same importance was considered for all responses; thus, multi-objective condition can simultaneously satisfy all of the requirements. Taguchi categorized performance characteristics into three different types, including the nominal the better, the smaller the better and the larger the better. In this study the smaller the better was selected to minimize all surface integrity characteristics responses and larger the better is selected for MRR. Table 14 shows conditions that are desirable to achieve best surface integrity characteristics with maximum MRR.

Table 12. Constraints for optimization of pre-treatment parameters.

Name	Goal	Lower limit	Upper limit	Lower weight	Upper weight	Importance
Pulse-on time (μs)	In range	2	12	1	1	3
Pulse-off time (μs)	In range	2	10	1	1	3
Peak current (A)	In range	8	40	1	1	3
Servo voltage	In range	20	50	1	1	3
White layer thickness	Minimize	3.764	6.015	1	1	3
Surface crack density	Minimize	0.0044	0.0488	1	1	3
Heat-affected zone	Minimize	3.216	4.7	1	1	3

Table 13. The optimal condition for each parameter.

Condition	Pulse-on time (μs)	Pulse-off time (μs)	Peak current (A)	Servo voltage(V)	Optimum response	Desirability
White layer thickness (μm)	2.5	5.5	11.5	30	3.106	1
Surface crack density (μm/μm ²)	7.5	2.5	15.25	50	0.0011957	1
Heat-affected zone (μm)	3.5	3.75	27	45	2.929	1
Material removal rate (mm ³ /s)	10.7	2.7	34	49	0.41	1
Multi-objectives	6.5	2	18.8	40.7		0.712

Table 14. The optimal condition for each parameter with maximum MRR.

Condition	Pulse-on time (μs)	Pulse-off time (μs)	Peak current (A)	Servo voltage (V)	Optimum response for WLT	Optimum response for MRR	Desirability
WLT (μm)	2	4.3	40	40	4.53	0.38	0.65
SCD (μm/μm ²)	8	2	18	44	0.01	0.373	0.734
HAZ (μm)	3.3	2	31	45	2.929	3.016	0.778

5. Conclusion

In this research the effects of machining parameters including pulse-on time, pulse-off time, peak current and servo voltage on surface integrity features such as HAZ, surface crack density and white layer thickness of Titanium (Ti-6Al-4V) were experimentally studied. Statistical optimized model (CCD coupled with RSM) overcomes the limitation of classical methods and it is used to obtain optimum process conditions.

The results of this study show that WEDM can be suitable for machining of Ti-6Al-4V if the machining parameters are optimized, which results in minimizing the surface integrity defections.

The following conclusions were obtained:

1. T_{on} was identified as the most significant factor influencing HAZ. This factor will affect the thermal stress expose to the workpiece in time, which is very important with respect to the low thermal conductivity of titanium. The percentage contribution of various parameters on HAZ has been found: pulse-on time, 66.64%; pulse-off time, 1.08%; peak current, 15.7% and servo voltage, 6.832%.
2. IP was found to be the most significant factor that affects surface crack density. Increasing the peak current also increases the energy of each discharge, producing wider and deeper craters, which can affect the tendency to produce crack in the surface. The contribution percentage of various parameters on surface crack density was found as follows: pulse-on time, 11.28%; pulse-off time, 0.79%; peak current, 74.89% and servo voltage, 4.15%.
3. IP was recognized as the most significant factor that affects white layer thickness. Also, T_{on} and SV play major roles on this response. The contribution percentage of different parameters on white layer thickness was found to be as follows: pulse-on time, 23.8%; pulse-off time, 4.22%; peak current, 29.17% and servo voltage, 15.66%.
4. IP was recognized as the most significant factor for MRR. The contribution percentage of different parameters on white layer thickness was found to be as follows: pulse-on time, 24.39%; pulse-off time, 3.2%; peak current, 42.04% and servo voltage, 23.39%.
5. IP is the most important factor for surface topology aspects, especially voids, surface and penetrating cracks,

while T_{on} affects other aspects such as surface porosity and debris.

6. The residuals of copper and zinc were identified in the machined samples using EDX analysis. This could be attributed to the transfer of zinc-coated brass wire electrode after decomposition to the work surface. The presence of oxygen in the titanium was due to vaporization of dielectric fluid (deionized water) and oxidation as a result of high temperature involved in the process.
7. Several optimal conditions were obtained from the analysis, including multi-objective condition, which can be set as pulse-on time = 6 μs, pulse-off time = 2 μs, peak current = 18 A and servo voltage = 50 V. The predicted results are surface crack density = 0.011 μm/μm², HAZ = 3.26 μm, white layer thickness = 4.99 μm and material removal rate = 0.25 mm³/s. Empirical equations to predict these responses are obtained and verified using confirmation tests and residual analysis.
8. It is possible to predict different responses in the optimum region of the procedure. Several optimal conditions may be obtained from the analysis, including the multi-objective conditions, which were set by pulse-on time = 6.55 μs, pulse-off time = 2 μs, peak current = 18.82 A and servo voltage = 40.69 V. Predicted results are WLT = 4.35 μm, SCD = 0.0078 μm/μm², HAZ = 3.34 μm and MRR = 0.26 mm³/s.

Furthermore, future studies can focus on the effect of other parameters such as workpiece thickness, wire tension and wire feed on surface integrity parameters.

Nomenclature

T_{on}	Pulse-on time
T_{off}	Pulse-off time
IP	Peak current
SV	Servo voltage
WLT	White layer thickness
HAZ	Heat-affected zone
SCD	Surface crack density
MRR	Material removal rate
RSM	Response surface methodology
FESEM	Field emission scanning electron microscope
EDX	Energy-dispersive X-ray
WEDM	Wire electrical discharge machining
ANOVA	Analysis of variance

References

- [1] Rao P V and Pawar P J 2009 Modelling and optimization of process parameters of wire electrical discharge machining. *Proc. IMechE Part B: J. Eng. Manuf.* 223: 1431–1440
- [2] Ho K H, Newman S T and Allen R D 2005 STEP-NC compliant information modelling for wire electrical discharge machining component. *Proc. IMechE Part B: J. Eng. Manuf.* 219: 777–784
- [3] Hsieh J F 2011 Modelling tool path in wire electric discharge machining using Denavit–Hartenberg notation. *Proc. IMechE Part B: J. Eng. Manuf.* 225: 1063–1072
- [4] Sarkar S, Ghosh K, Mitra S and Bhattacharyya B 2010 An integrated approach to optimization of WEDM combining single-pass and multipass cutting operation. *Mater. Manuf. Process.* 25(8): 799–807
- [5] Ghodsiyeh D, Golshan A and Shirvanehdeh J A 2013 Review on current research trends in wire electrical discharge machining (WEDM). *Indian J. Sci. Technol.* 6(2): 154–168
- [6] Boyer H E and Gall T L 1985 *Metals handbook*. Metals Park, Ohio: ASM Int., pp. 9.1–9.12
- [7] Donachie Jr. M J 2000 *Titanium – a technical guide*, 2nd ed. Ohio: ASM Int., pp. 318–323
- [8] Goswami A and Kumar J 2014 Investigation of surface integrity, material removal rate and wire wear ratio for WEDM of Nimonic 80A alloy using GRA and Taguchi method. *Eng. Sci. Technol. Int. J.* 17: 173–184
- [9] Newton T R, Melkote S N, Watkins T R, Trejo R M and Reister L 2009 Investigation of the effect of process parameters on the formation and characteristics of recast layer in wire-EDM of Inconel 718. *Mater. Sci. Eng. A* 513–514: 208–215
- [10] Kumar A, Kumar V and Kumar J 2013 Multi-response optimization of process parameters based on response surface methodology for pure titanium using WEDM process. *Int. J. Adv. Manuf. Technol.* 68(9–11): 2645–2668
- [11] Kumar A, Kumar V and Kumar J 2014 Surface integrity and material transfer investigation of pure titanium for rough cut surface after wire electro discharge machining. *Proc. IMechE Part B: J. Eng. Manuf.* 228(8): 880–901
- [12] Kumar A, Kumar V and Kumar J 2013 Investigation of machining parameters and surface integrity in wire electric discharge machining of pure titanium. *Proc. IMechE Part B: J. Eng. Manuf.* 227(7): 972–992
- [13] Puri A B and Bhattacharyya B 2005 Modeling and analysis of white layer depth in a wire-cut EDM process through response surface methodology. *Int. J. Adv. Manuf. Technol.* 25: 301–307
- [14] Kumar A, Kumar V and Kumar J 2016 Surface crack density and recast layer thickness analysis in WEDM process through response surface methodology. *Mach. Sci. Technol. Int. J.* 20(2): 201–230
- [15] Garg M P, Kumar A and Sahu C K 2017 Mathematical modeling and analysis of WEDM machining parameters of nickel-based super alloy using response surface methodology. *Sadhana* 42(6): 981–1005
- [16] Golshan A, Ghodsiyeh D and Izman S 2015 Multi-objective optimization of wire electrical discharge machining process using evolutionary computation method: effect of cutting variation. *Proc. IMechE Part B: J. Eng. Manuf.* 229(1): 75–85
- [17] Padhee S, Nayak N, Panda S K, Dhal P R and Mahapatra S S 2012 Multi-objective parametric optimization of powder mixed electro-discharge machining using response surface methodology and non-dominated sorting genetic algorithm. *Sadhana* 37(2): 223–240
- [18] Montgomery D C 2009 *Design and analysis of experiments*, 7th ed. Singapore: John Wiley & Sons, pp. 207–264
- [19] Lee H T and Tai T Y 2003 Relationship between EDM parameters and surface crack formation. *J. Mater. Process. Technol.* 142: 676–683
- [20] Noordin M Y, Venkatesh V C, Sharif S, Elting S and Abdulla A 2004 Application of response surface methodology in describing the performance of coated carbide tools when turning AISI 1045 steel. *J. Mater. Process. Technol.* 145: 46–58
- [21] Routara B, Bandyopadhyay A and Sahoo P 2009 Roughness modeling and optimization in CNC end milling using response surface method: effect of workpiece material variation. *Int. J. Adv. Manuf. Technol.* 40: 1166–1180
- [22] Sarkar S, Mitra S and Bhattacharyya B 2005 Parametric analysis and optimization of wire electrical discharge machining of γ -titanium aluminide alloy. *J. Mater. Process. Technol.* 159: 286–294
- [23] Kanlayasiri K and Boonmung S 2007 Effects of wire-EDM machining variables on surface roughness of newly developed DC 53 die steel: design of experiments and regression model. *J. Mater. Process. Technol.* 192–193: 459–464
- [24] Kanlayasiri K and Boonmung S 2007 An investigation on effects of wire-EDM machining parameters on surface roughness of newly developed DC53 die steel. *J. Mater. Process. Technol.* 187–188: 26–29
- [25] Lee S H and Li X P 2003 Study of the surface integrity of the machined workpiece in the EDM of tungsten carbide. *J. Mater. Process. Technol.* 139: 315–321
- [26] Hascalik A and Caydas U 2007 Electrical discharge machining of titanium alloy (Ti–6Al–4V). *Appl. Surf. Sci.* 253: 9007–9016
- [27] Ghodsiyeh D, Golshan A and Izman S 2014 Multi-objective process optimization of wire electrical discharge machining based on response surface methodology. *J. Braz. Soc. Mech. Sci.* 36(2): 301–313
- [28] Sadeghi M, Razavi H, Esmaeilzadeh A and Kolahan F 2011 Optimization of cutting conditions in WEDM process using regression modelling and Tabu-search algorithm. *Proc. IMechE Part B: J. Eng. Manuf.* 225: 1825–1834
- [29] Tosun N and Cogun C 2003 Analysis of wire erosion and workpiece surface roughness in wire electrical discharge machining. *Proc. IMechE Part B: J. Eng. Manuf.* 217: 633–642
- [30] Tzeng C J, Yang Y K, Hsieh M H and Jeng M C 2011 Optimization of wire electrical discharge machining of pure tungsten using neural network and response surface methodology. *Proc. IMechE Part B: J. Eng. Manuf.* 225: 841–852
- [31] Jia Y, Kim B S, Hu D J and Ni J 2010 Parametric study on near dry wire electro discharge machining of polycrystalline diamond-coated tungsten carbide material. *Proc. IMechE Part B: J. Eng. Manuf.* 224: 185–193
- [32] Hascalik A and Caydas U 2004 Experimental study of wire electrical discharge machining of AISI D5 tool steel. *J. Mater. Process. Technol.* 148: 362–367